Available online at www.sciencedirect.com

ScienceDirect

Solar Energy 111 (2015) 297–312

SOLAR ENERGY

www.elsevier.com/locate/solener

# Master optimization process based on neural networks ensemble for 24-h solar irradiance forecast

C. Cornaro [a,b,*], M. Pierro [a], F. Bucci [a]

[a] Department of Enterprise Engineering, University of Rome Tor Vergata, Via del Politecnico, 1 00133 Rome, Italy
[b] CHOSE, University of Rome Tor Vergata, Via del Politecnico, 1 00133 Rome, Italy

Received 3 March 2014; received in revised form 10 October 2014; accepted 24 October 2014

Communicated by: Associate Editor David Renne

**Abstract**

In the paper two models implemented to forecast the hourly solar irradiance with a day in advance are described. The models, based on Artificial Neural Networks (ANN), are generated by a master optimization process that defines the best number of neurons and selects a suitable ensemble of ANN.

The two models consist of a Statistical (ST) model that uses only local measured data and a Model Output Statistics (MOS) that corrects Numerical Weather Prediction (NWP) data. ST and MOS are tested for the University of Rome "Tor Vergata" site. The models are trained and validated using one year data. Through a cross training procedure, the dependence of the models on the training year is also analyzed.

The performance of ST, NWP and MOS models, together with the benchmark Persistence Model (PM), are compared. The ST model and the NWP model exhibit similar results. Nevertheless different sources of forecast errors between ST and NWP models are identified. The MOS model gives the best performance, improving the forecast of approximately 29% with respect to the PM.


*Keywords:* Solar irradiance; Forecast; Neural network; MOS; Ensemble

## 1. Introduction

The rapid growth of electricity produced by PV has introduced some criticisms into the grid due to the fluctuating nature of energy source which is dependent on meteorological conditions. Thus reliable forecast models are required for management and operation strategies. In particular the 24/72 h horizon forecast is essential for transmission scheduling and day ahead energy market. In Italy the PV energy production during the 2012 reached 18.9 GW h produced by 16.4 GW installed providing an average of 7% of yearly electrical consumption with a monthly peak of 9% (Statistical data from the Italian Manager of Electrical Services (GSE): "Solare Fotovoltaico - Rapporto Statistico 2012" and Statistical data from the Italian Manager of the National Electrical Transmission Grid: "produzione 2012").

The techniques to forecast the solar radiation or PV production on the 24/72 h horizon can be divided in three mains groups:

(1) Numerical Weather Prediction models (NWP)
(2) Statistical models (ST)
(3) Model Output Statistic (MOS)

* Corresponding author at: Department of Enterprise Engineering, University of Rome Tor Vergata, Via del Politecnico, 1 00133 Rome, Italy. Tel.: +39 0672597233.
*E-mail address:* cornaro@uniroma2.it (C. Cornaro).

http://dx.doi.org/10.1016/j.solener.2014.10.036
0038-092X/

**Nomenclature**

*Abbreviations*

| | |
|---|---|
| NWP | Numerical Weather Prediction model |
| ST | Statistical model |
| MOS | Model Output Statistic model |
| ANN | Artificial Neural Network |
| MLP NN | Multi-Layer Perceptron Neural Network |
| STNN | Developed Statistical model based on ANN |
| ECMWF-MOSNN | Developed Model Output Statistic model based on ANN and ECMWF NWP data |

*Variables and dimensions*

| | |
|---|---|
| $Gh$ | Global Horizontal Irradiance W/m$^2$ |
| Gpoa | Global Irradiance on the Plane of Array W/m$^2$ |
| NADV | Normalized Absolute Daily Variation of the solar radiation between the day ($t$) and the day ($t-1$) Dimensionless |
| NMHV | Normalized Maximum Hourly Variation of the solar irradiance Dimensionless |
| $K_t$ | Clearness index Dimensionless |
| $P_{\text{index}}$ | persistence index Dimensionless |
| Hh | daily horizontal irradiation W h/m$^2$ day |
| Ta | average daily temperature °C |
| OD | Ordinal Day number Dimensionless |
| $H_{\text{NWP}}$ | Daily irradiation forecast W h/m$^2$ day |
| $Gh_{cs}$ | Clear Sky Global Horizontal Irradiance (Ineichen/Perez model) W/m$^2$ |
| $P(X)$ | quantile trajectory W/m$^2$ |
| MSE | Mean Square Error (W/m$^2$)$^2$ |
| Corr | Pearson correlation index Dimensionless |
| RMSE | Root Mean Square Error W/m$^2$ |
| MAE | Mean Absolute Error W/m$^2$ |
| MBE | Mean Bias Error W/m$^2$ |
| Irmse | skill score with respect to the RMSE metric Dimensionless |
| $\Delta G_{\text{rel}}$ | mean width of the prediction intervals W/m$^2$ |

The numerical weather prediction models are essentially based on the numerical integration of coupled differential equations that describe the dynamics of the atmosphere and radiation transport mechanisms. The main advantage of these forecasting methods is that they are based on deterministic physical models. On the other hand, the main problem, in addition to the non-linearity of the used equations, is the spatial resolution of the integration grid: from 100 km (Global models) to few km (Mesoscale models) that is too wide with respect to the PV plants size. Inside the grid cell the cloud cover and aerosols are homogeneously fixed at their average values thus great errors could be induced both in the amount and in the time of the forecast irradiance on the PV site. Besides many NWP models have a temporal output interval greater than one hour while, as in this case, the hourly irradiance forecast is required. A comparison of main numerical weather prediction models (Global and Mesoscale models) for solar irradiance forecast in different locations can be found in Perez et al. (2010, 2013) and Muller and Remund (2010).

The statistical models are based on methods to reconstruct the relations between the hourly irradiance and past meteorological parameters (cloud ratio, air temperature, relative humidity, pressure, etc.) or past irradiance observations. The most used models for the one day horizon irradiance forecast are based on Artificial Neural Networks (ANN). Thus spatial and temporal resolution problems are overcome since these methods use ground measurements taken directly on the PV plant site with a temporal resolution less than one hour. On the other hand these methods are not able to provide a good forecast in unstable weather conditions since in these cases the correlation between the irradiance and the meteorological variables rapidly falls down. Several statistical models for 24 h forecast of global irradiance or PV power can be found in the literature presenting different ANN architectures. In Di Piazza et al. (2013) and Chaouachi et al. (2009) time series ANN Focused Time-Delay Neural Network (FTDNN) and the Nonlinear Autoregressive Network with exogenous inputs (NARX Network), are used. Radial Basis Function Neural Network (RBFNN) is also implemented in Chaouachi et al. (2009), while Multi-Layer Perceptron Neural Network (MLPNN) are developed in Chaouachi et al. (2009), Mellit and Massi (2010) and Voyant et al. (2013).

The model output statistics approach combines both NWP and ST models. The first one is used for the forecast while the second is used to correct the site effects through local ground measurements. The ST models are essentially used to down scale the irradiance forecast, reducing the systematic errors of the physical models. A variety of model output statistic models that use statistical post processing of the NWP output and stochastic learning techniques have been developed by various authors. In Perotto et al. (2013) a post-processing algorithm to correct the radiation schemes used by the WRF-NWP model is described. This is a physical based algorithm that improves the forecast of atmosphere water vapor profile. It uses regression coefficients that should be calculated from ground measurements. A statistical post-processing correction of the bias errors of the ECMWF-NWP data was proposed by Lorenz et al. (2009a). This seems to be the most performing MOS model for global irradiance forecast (Lorenz et al., 2009b). Perez et al. (2007) developed a semi empirical model that correlates the NWP sky cover (provided by the National Digital Forecast Database, USA) with the global horizontal irradiance.

The advantage of the MOS models that use stochastic learning techniques, is that they can easily use NWP data to provide a direct forecast of a different variable (Marquez and Coimbra, 2011; Chen et al., 2011; Wang et al., 2011; Huang et al., 2010; Cai et al., 2010; Cao and Lin, 2008 and Yona et al., 2008). In Marquez and Coimbra (2011), Huang et al. (2010) and Yona et al. (2008) the MLPNN were used, and in Wang et al. (2011) this ANN architecture was coupled with the Gray Model. The RBFNN is developed in Chen et al. (2011) and Yona et al. (2008) while NARX in Cai et al., 2010, Recurrent Neural Networks (RNN) and Diagonal Recurrent Wavelet Neural Networks (DRWNN) were implemented in Cao and Lin (2008) and Yona et al. (2008).

An overview on solar irradiance and PV power forecast techniques could be found in Paulescu et al. (2013), Kleissl (2013) and Photovoltaic and Solar Forecasting: State of the Art. IEA PVPS Task 14 (2013), while a complete study on solar radiation benchmarks is reported in Lorenz et al. (2009b), Beyer et al. (2009) and Traunmüller and Steinmaurer (2010).

To the author knowledge few works have been found in the literature about solar irradiance forecast for Italy (Mellit and Massi, 2010 and Di Piazza et al., 2013). Moreover no benchmark cases were found for the same country. This work contributes to fill this gap providing a benchmark for the Rome site, obtained with four years data analysis.

Besides, although the use of the ensemble technique is very well known and applied in the weather forecast community, this method has not yet been extensively explored for the solar irradiance forecast through NWP or ANN approaches.

The aim of the work presented in the paper was:

1. To develop two models (ST and MOS) for the 24 h forecast of global horizontal irradiance based on an ensemble of Artificial Neural Networks (ANN). The ensemble was generated through an automatic procedure called master optimization process (Photovoltaic and Solar Forecasting: State of the Art. IEA PVPS Task 14, 2013).
2. To analyze the dependency of the models on the dataset used to train and validate the ANN. Thus a cross training procedure was adopted.
3. To identify the main sources of error of NWP, ST and MOS models.
4. To evaluate the ST and MOS models performance with respect to the NWP and the persistence model (used as a benchmark), for the site of Rome "Tor Vergata" and the years from 2008 to 2011. The reported performance results from the average of the yearly performance of three models (each trained on a different year dataset). In this way the performance does not depend on the training year any more.

In Section 2, local measurements and NWP data used to train and to test the models are presented. In Section 3 the irradiance site characterization parameters used to analyze the model performance are reported. In Section 4, the methodology adopted to develop the forecasting model is described in detail. Section 5 summarizes the metrics used to evaluate the forecast performance and the persistence model used as a benchmark. In Section 6 the reliability of the models in terms of dependence on training dataset is studied. In Section 7 the source of errors of NWP and ST models are analyzed to explain why the MOS model, that combines the deterministic and statistic approaches, shows the best performance. Finally in Section 8 models performance is analyzed with respect to the irradiance site characterization parameters and compared with the accuracy obtained by other forecast models in different EU countries (Lorenz et al., 2009b).

## 2. Data description

### 2.1. Local experimental data and pre-processing

The local experimental data used as input and to train and test the models come from the ESTER outdoor Laboratory – University of Rome "Tor Vergata" (Spena et al., 2008). The global horizontal irradiance and the air temperature are measured every minute, from January 2008 to the end of December 2011 using a secondary standard pyranometer CM21 by Kipp and Zonen and a Platinum resistance thermometer (PT100). The data were filtered removing not physically consistent measurements due to monitoring problems. For each day, if no more than 60 consecutive missing samples were encountered, a data reconstruction by linear interpolation was applied. Otherwise, if more than 60 consecutive missing samples were found the whole day was removed from the data set. After this operation the hourly and monthly data were calculated.

The data reconstruction was introduced to overcome the data monitoring system problems yield in underestimation of the incident irradiance.

### 2.2. NWP data

The NWP data used come from the European Centre for Medium-Range Weather Forecasts (ECMWF), an intergovernmental organization supported by 34 States that provides forecasts mainly for scientific purposes. The data collected from the repository MARS (Meteorological Archival and Retrieval System) belong to the database called ERA-Interim, Atmospheric Model, Forecast that is a reanalysis of the atmospheric global covering since 1979. The data taken, identified with id 169 short name

‘SSRD’ according to the table ECMWF128, correspond to the surface solar radiation downwards; the aggregate value comes every 3 hours starting from 00:00 (UTC). The spatial resolution of these data correspond to a cell of 13.5 km × 13.5 km side (0.125° × 0.125°), the maximum available resolution. To obtain the hourly irradiance, a linear interpolation over the average 3 h irradiance was performed. The same procedure was also used in Lorenz et al. (2009a). According to the local measurements the considered period is between the 1 January 2008 and 31 December2011.

## 3. Irradiance site characterization parameters

To characterize the irradiance in the specific site and year, three main parameters are used:

- NADV = Normalized Absolute Daily Variation of the solar radiation between the day ($t$) and the day ($t-1$).
- NMHV = Normalized Maximum Hourly Variation of the solar irradiance.
- $K_t$ = clearness index.

NADV and NMHV are introduced in this paper by the authors while the $K_t$ is a commonly used indicator.

### 3.1. Normalized daily variation and normalized absolute daily variation

The normalized daily variation and normalized absolute daily variation of the solar irradiation are defined as:

$$\mathrm{NDV} = \frac{(H(t) - H(t-1))}{\frac{H(t) + H(t-1)}{2}} \ (-);$$

$$\mathrm{NADV} = |\mathrm{NDV}| \ (-) \tag{1}$$

where $H(t)$ and $H(t-1)$ = irradiation at days $t$ and $t-1$.

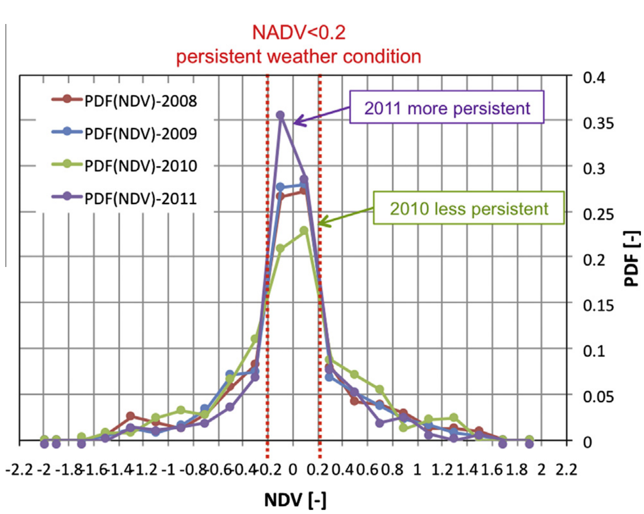


Fig. 1. PDF of NDV of the horizontal irradiation of four years in Rome.

NADV is an indicator of the persistence of the weather conditions since it measures the daily irradiation variation of one day with respect to the previous one. Thus, days with NADV < 0.2 are considered belonging to stable weather conditions. Fig. 1 shows the Probability Density Function (PDF) of NDV of the horizontal irradiation.

It can be observed that small variations of weather conditions between two consecutive days (low NADV) are much more probable than fast weather changing (high NADV). In Rome during the reference period the probability of stable weather conditions changes from 44% in 2010 (less persistent year) to 64% in 2011 (more persistent year). In a specific year and site the tendency of the weather conditions to remain the same could be characterized by the mean value of NADV (mean(NAVD)) and by the standard deviation of NDV (std(NDV)). Lower values of these parameters indicate persistent weather conditions. Fig. 2 shows that there is a strong linear correlation between the persistence index, defined by Eq. (2), and the Normalized Mean Absolute Error (NMAE) obtained by the simplest version of persistence model, see Eq. (3).

$$P_{\mathrm{index}} = \mathrm{Mean}(\mathrm{NADV}) * \mathrm{Std}(\mathrm{NDV}) \tag{2}$$

$$\mathrm{NMAE} = \frac{\sum_{i=1}^{n} |G_i^m - G_i^{\mathrm{Persistence}}|}{\sum_{i=1}^{n} G_i^m} \ (\%) \tag{3}$$

where

$G_i^m$ = measured hourly irradiance (W/m$^2$).

$G_i^{\mathrm{Persistence}}$ = 24 h irradiance forecast obtained by the persistence model (W/m$^2$).

This simple version of persistence model just assumes that the irradiance of the day ($t+1$): $[G_1^{\mathrm{Persistence}}(t+1) \ldots G_{24}^{\mathrm{Persistence}}(t+1)]$ is equal to the measured irradiance of the day ($t$): $[G_1^m(t) \ldots G_{24}^m(t)]$.

The good correlation proves that NADV is a good indicator of weather persistence and the annual forecast error of the persistence model can be easily estimated using the $P_{\mathrm{index}}$.

### 3.2. Normalized maximum hourly variation

The normalized maximum hourly variation of the solar irradiance is defined as:

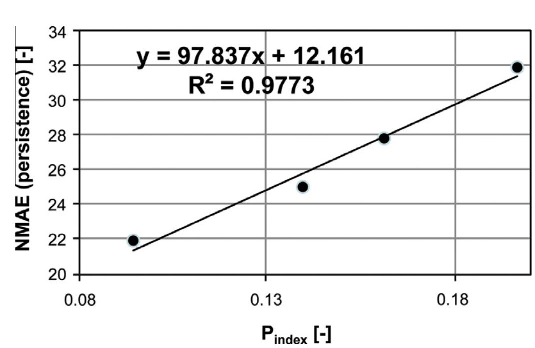


Fig. 2. Correlation of the $P_{\mathrm{index}}$ and the NMAE of the persistence model.

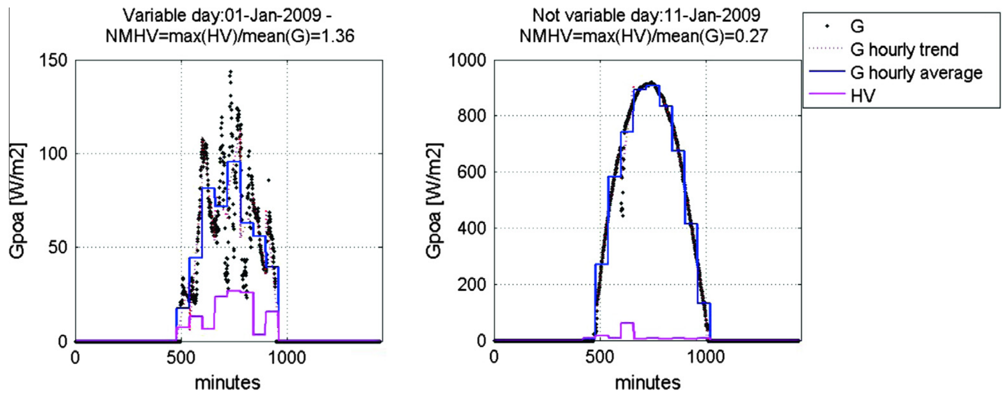


Fig. 3. Gpoa = Global Irradiance on the Plane of Array. (Left) variable irradiance day NMHV = 1.36; (right) stable irradiance day NMHV = 0.27.

$$\mathrm{NMHV} = \frac{\max_h\left\{\sqrt{\frac{\sum_{\min=1}^{60}(G_h^{\min}-fit(G_h^{\min}))^2}{60}}\right\}}{\langle G_h^{\min}\rangle_{\mathrm{day}}}\ (-) \tag{4}$$

where $G_h^{\min}$ = irradiance at minute (min) of the hour $(h)\left(\frac{\mathrm{W}}{\mathrm{m}^2}\right)$, $\mathrm{fit}(G_h^{\min})$ = irradiance at minute (min) obtained by the hourly linear fit of $G_h^{\min}\left(\frac{\mathrm{W}}{\mathrm{m}^2}\right)$ and $\langle G_h^{\min}\rangle_{\mathrm{day}}$ = daily average irradiance$\left(\frac{\mathrm{W}}{\mathrm{m}^2}\right)$.

Defining the irradiance measured with one minute time rate during an hour ($h$) as the set $\{G_h^{\min}\}_{\min=1:60}$, the linear fit of $\{G_h^{\min}\}$ describes the hourly trend of the measured irradiance. Thus the root mean square error between the measured irradiance and the one obtained by the linear fitting: $\mathrm{HV} = \sqrt{\frac{\sum_{\min=1}^{60}(G_h^{\min}-\mathrm{fit}(G_h^{\min}))^2}{60}}$, represents the variation of the irradiance with respect to the hourly trend. Fig. 3 shows the hourly variations (HV) for a variable and a not variable day. During clear sky days these variations are very small (see magenta line in the right picture of Fig. 3), on the contrary during variable irradiance days the HV reaches higher values (see magenta line in the left picture of Fig. 3).

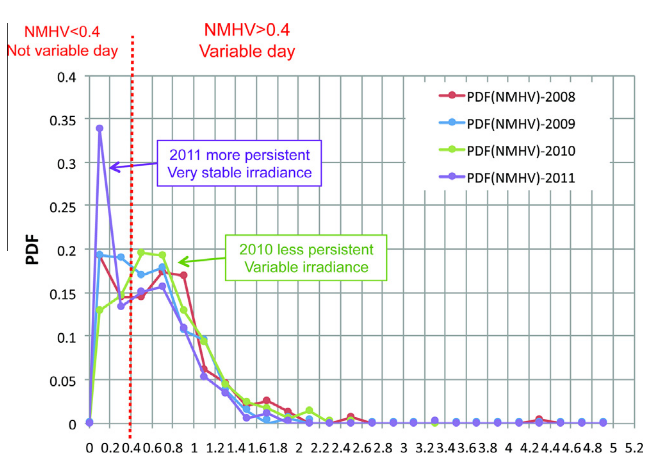


Fig. 4. PDF of NMHV of the horizontal irradiation of four years in Rome.

Thus the NMHV statistical parameter represents the maximum fluctuation of the measured irradiance around the hourly trend with respect to the daily average irradiance and it can be used to describe the daily variability of the irradiance. In clear sky days it is near to zero while in overcast days it could reach the value of five (the daily maximum variation is 5 times the mean daily irradiance).

Fig. 4 shows the PDF of NMHV of the horizontal irradiation. NMHV < 0.4 has been considered as indicator of days with stable irradiance conditions. It can be observed that the year with more persistent weather conditions (2011) has much more stable irradiance days with respect to other years.

### *3.3. Clearness index*

The Clearness Index is a well known parameter and it is defined as the ratio between the horizontal daily irradiation ($H$) and the extraterrestrial horizontal irradiation ($H_{\mathrm{ext}}$):

$$K_t = \frac{H}{H_{\mathrm{ext}}}\ (-) \tag{5}$$

It is strictly related to the stochastic meteorological conditions: days with $K_t$ greater than 0.7 are considered clear sky days, with $K_t$ between 0.3 and 0.7 are considered partly cloudy while days with $K_t$ lower than 0.3 are considered overcast days. Fig. 5 shows the PDF of $K_t$ for the reported period. It can be pointed out that year with more persistent weather conditions (2011) has much more clear sky days with respect to other years.

## 4. Methodology

### *4.1. Description of the models*

To develop the ST and MOS models, the Multi-Layer Perceptron Neural Network architecture (MLPNN), with one hidden layer, was used. This architecture, synthetically reported in Fig. 6, uses meteorological parameters to forecast the one day ahead hourly irradiance:

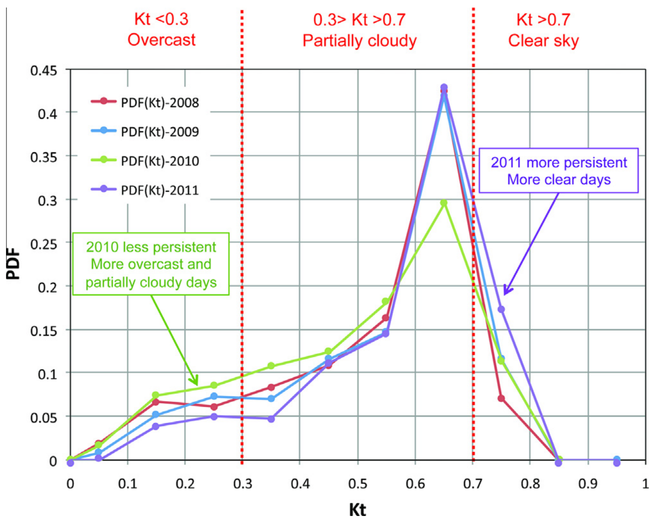


Fig. 5. PDF of clearness index ($K_t$) of four years in Rome.

$$[Gh_1(t+1), \ldots Gh_{24}(t+1)] = f(\text{meteorological parameters}) \quad (6)$$

The input meteorological parameters come only from past local measurements (in the case of the ST model) while in the case of the MOS models also NWP variables are used as input.

### 4.2. Input meteorological parameters

A variety of meteorological parameters, coming from ground measurements (for ST models) and NWP products (for MOS model), has been used in the literature as input of MLPNN. Among these meteorological parameters it can be evidenced: the daily average temperature (Chaouachi et al., 2009; Mellit and Massi, 2010 and Wang et al., 2012); the max and min daily temperature, the daily average humidity, the vapor pressure, the cloud cover, the sunshine duration (Chaouachi et al., 2009); the hourly irradiance (Chaouachi et al., 2009) and the daily average irradiance (Wang et al., 2012); pressure, nebulosity and precipitation (Voyant et al., 2013), zenith angle (Marquez and Coimbra, 2011; Huang et al., 2010). From the NWP forecast variables, it can be found: sky cover (defined as the expected amount of opaque clouds, in percent, covering the sky, valid for the indicated hour), probability of precipitation, minimum temperature (Marquez and Coimbra, 2011), daily average temperature (Huang et al., 2010; Yona et al., 2008) and irradiance (Huang et al., 2010).

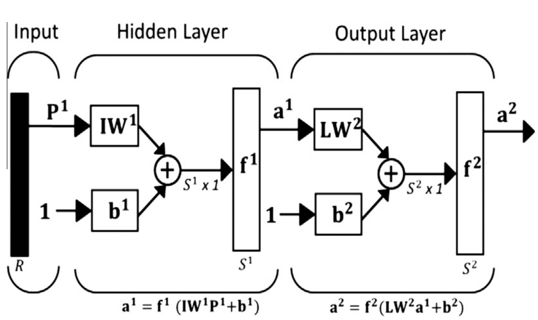


Fig. 6. Sketch of the MultiLayer Perceptron Neural Network (MLPNN) architecture. $\mathbf{P^1}$: input vector with $R$ rows. For $i$-layer, $\mathbf{IW^i}$: input weights, $\mathbf{LW^i}$: layer weights, $\mathbf{b^i}$: bias vector, $\mathbf{S^i}$: number of neurons, $\mathbf{a^i}$: output vector, $\mathbf{f^i}$: transfer function ($f^1$ = tansigmoid, $f^2$ = pureline).

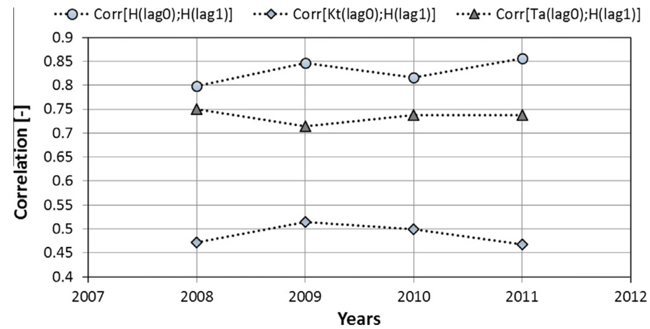


Fig. 7. Pearson correlation between the input parameters measured at day $t$ and the irradiation ($H$) measured at day $t+1$, for the considered period.

In particular it should be underlined that Wang et al. (2012) used also two statistical parameters similar to the above reported NDV and NMHV as input of their NN model. In the present case, worst forecasting accuracy was found including these input parameters. In Voyant et al. (2013) a statistical investigation of different possible input variable was performed, while in Marquez and Coimbra (2011) a Gamma test combined with a Genetic Algorithm were used to select the best NWP input set for their MOS.

Since the final objective of the work is to forecast the PV energy production, all the inputs of the reported forecasting models should be variables that are commonly measured by the medium–large size PV plant monitoring systems. On the other hand, as pointed out in Voyant et al. (2013), the input meteorological parameters measured at the present day ($t$) should be strongly correlated with the irradiation of the next day ($t+1$). Thus the Ordinal Day number (OD, defined as the day of year ranging from 1 to 366), the daily irradiation ($H$), the average daily temperature ($Ta$) and the clearness index ($K_t$) measured at time $t$ have been chosen as input of the MLPNN models. Fig. 7 shows the Pearson correlation (Eq. (7)) between the daily irradiation ($H$) measured at day $t+1$ and the daily irradiation ($H$), the average daily temperature ($Ta$), the clearness index ($K_t$) measured at day $t$.

The Ordinal Day number (OD) has been included since it takes into account the astronomical information (such as the yearly variations of sunrise and sunset hours). For the MOS model also the daily irradiation forecast ($H_{NWP}$) provided by the ECMWF database, was used as input of the neural network. The models were developed using the ANN MatLab Toolbox.

Fig. 8 summarizes the basic feature and the nomenclature of the two MLPNN architectures used for the forecasting models.

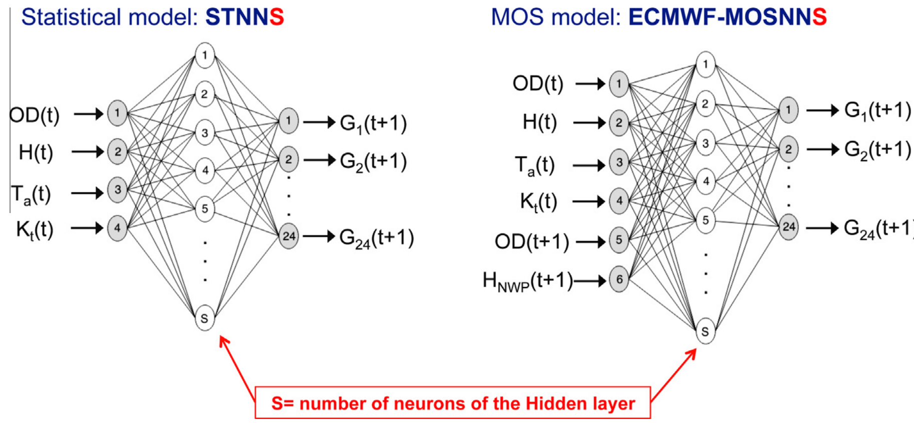


Fig. 8. Statistical model NN architecture (STNNS) and MOS model NN architecture (ECMWF-MOSNNS). The number $S$ indicates the optimal number of neuron in the hidden layer coming from the master optimization process.

### 4.3. Master optimization process

#### 4.3.1. Research of the optimal number of neurons of the hidden layer

The first step of the procedure was to automatically define the optimal number of neurons of the hidden layer ($S_{\text{optimal}}$).

For each $S$ (that goes from 1 to 40) the Repeated Random Sub-sampling Validation procedure (RRSV), described in Fig. 9, is repeated one hundred times ($N = 100$). It was tested that the partition of one year data sample into 60% days for training and 40% of days for validation was the one that produced the best performing model. The same result was found in Marquez and Coimbra (2011).

After the RRSV procedure, the performance of the MLP with S neurons was evaluated through the average value of the Mean Square Error MSE(i) over all the 100 iterations: MSEavg(S). From Fig. 10, it appears that for these models, the MSEavg(S) has a minimum. On the other hand, it is well know that the ANN loses its ability of generalization when the number of neurons is increased. Thus, between all the ANNs that have a MSEavg(S) near the minimum (below a fixed threshold), the optimal model is the one that has the minimum number of neurons ($S_{\text{optimum}}$). In the present case a threshold of 1% above the minimum of MSEavg was chosen.

The optimal number of neurons in the hidden layer for the STNN model was found between 5 and 8 while for the MOSNN model between 6 and 14, depending on yearly data set used for training and validation.

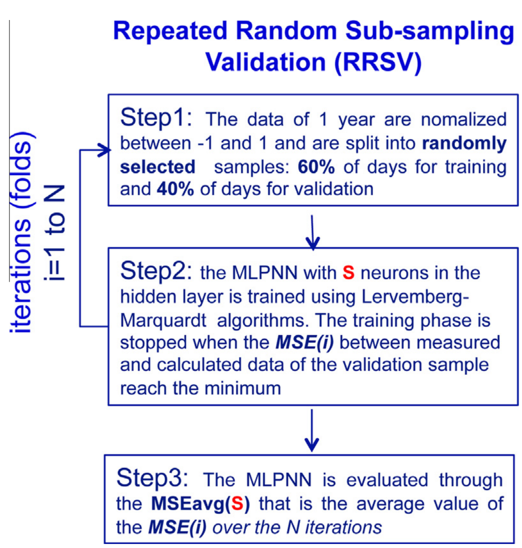


Fig. 9. RRSV procedure scheme.

#### 4.3.2. Generation and selection of a qualified ANN Ensemble

Once the best number of neurons ($S_{\text{optimum}}$) was identified, the second step of the procedure consisted in the ANN optimization. Iterating the RRSV procedure five hundred times, 500 ANNs were generated. Instead of choosing the $\text{ANN}_{\text{optimal}}$ as the one who showed an MSE(i) $\cong$ MSEavg, a qualified ensemble of ANN was selected. It was found that the best ensemble should contain all the ANN with a MSE(i) below the MSEavg (see Fig. 11). Each Neural Network in the Ensemble is a predictor and the result of each predictor on the test year data is a forecasting trajectory. The ensemble result is the average of all the predictor trajectories. The average over the ensemble tends to mitigate the noise produced by each predictor, resulting in a much more regular trajectory that better fits the experimental data.

This ensemble mean trajectory improved the performance from 0.5% to 2.5% with respect to the performance of the $\text{ANN}_{\text{optimal}}$, depending on the persistence of the weather. The less persistent is the test year, the greater is the ensemble performance improvement. For each model the number of ANN that belongs to the selected ensemble is around 300–350 ANN. Similar results were found in Chaouachi et al. (2009), but the potentiality of this technique was not completely investigated.

Moreover the ensemble technique allowed to calculate the quantile trajectories [$P(5),\ldots P(100)$]: for each hour of the test year, the experimental Cumulative Distribution

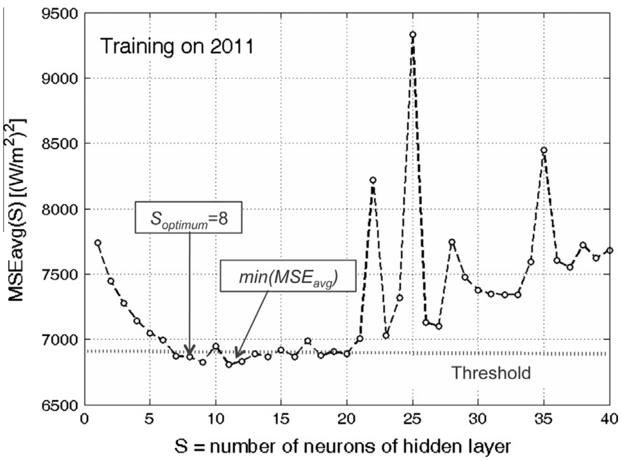


Fig. 10. The mean MSE realized during the RRVS procedure vs the number of the hidden layer neurons (S).

Function (CDF) was calculated so that the P(50) point is the value $Gh(50)$ such that the probability of $Gh \leqslant Gh(50)$ is equal to 50%. The quantile trajectories could be used also to correct systematic errors of the model. For example, Fig. 12 shows an underestimation at high irradiance level and an overestimation at low irradiance. It was verified that the $P(60)$ trajectory was able to reduce this model error, providing an outperforming forecast with respect to the mean trajectory. For this reason, in the present case, the $P(60)$ trajectory was used.

#### *4.3.3. Prediction intervals*

Through quantile trajectories it is possible to estimate the confidence interval of the prediction, so that the irradiance has the 95% of probability to be between the $P(5)$ and the $P(100)$ curves. In Fig. 13 it can be noted that for clear sky days the distance between the trajectory $P(5)$ and $P(100)$ is smaller than the one predicted for partially cloudy and overcast days.

Similar behavior of the forecasting errors was found in Lorenz et al. (2009a) and Marquez and Coimbra (2011) using a different way to estimate the forecasting uncertainty. Indeed, the authors assume a normal distribution of the residuals, with zero expected value and a site dependent variance.

## 5. Accuracy metrics and benchmarking model

According to the solar irradiance forecast literature, the following metrics are used to evaluate the models performance:

1. Pearson correlation index

$$\mathrm{Corr} = \frac{\sum_{i=1}^{n}(G_i^m - \overline{G^m})(G_i^f - \overline{G^f})}{\sqrt{\sum_{i=1}^{n}(G_i^m - \overline{G^m})^2 \sum_{j=1}^{n}(G_j^f - \overline{G^f})^2}} \quad (-) \tag{7}$$

2. Root mean square error

$$\mathrm{RMSE} = \frac{\sqrt{\sum_{i=1}^{n}(G_i^m - G_i^f)^2}}{n} \left(\frac{\mathrm{W}}{\mathrm{m}^2}\right) \tag{8}$$

3. Mean absolute error

$$\mathrm{MAE} = \frac{\sum_{i=1}^{n}\left|G_i^m - G_i^f\right|}{n} \left(\frac{\mathrm{W}}{\mathrm{m}^2}\right) \tag{9}$$

4. Mean bias error

$$\mathrm{MBE} = \frac{\sum_{i=1}^{n}\left(G_i^m - G_i^f\right)}{n} \left(\frac{\mathrm{W}}{\mathrm{m}^2}\right) \tag{10}$$

where $G_i^m$ = measured hourly irradiance (W/m$^2$) and $G_i^f$ = forecasted hourly irradiance (W/m$^2$).

The RMSE accentuates the greater forecasting errors while the MAE is exactly the measure of the unbalanced energy with respect to the total PV electricity fed into the grid. Bias error describes systematic deviation of the forecast. The normalized error indexes: NRMSE, NMAE and NMBE are calculated dividing by the measured irradiance averaged over the considered period. All the above performance indices are calculated excluding the night values.

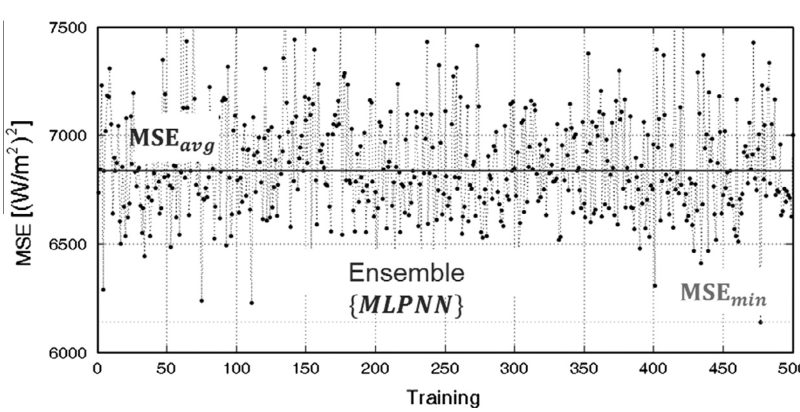


Fig. 11. Ensemble selection procedure.

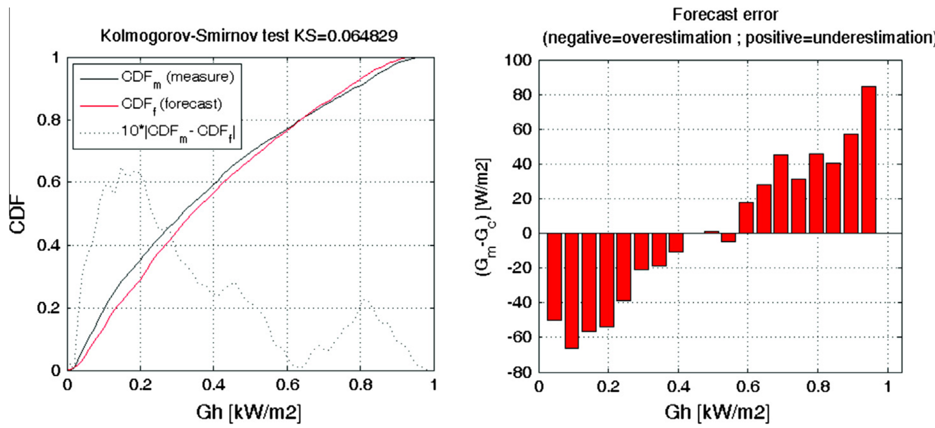


Fig. 12. Kolmogorov–Smirnov test and mean bias error of the $P(50)$ ECMWF-MOSNN14Tr2011 model (trained on 2011) tested on the 2010.

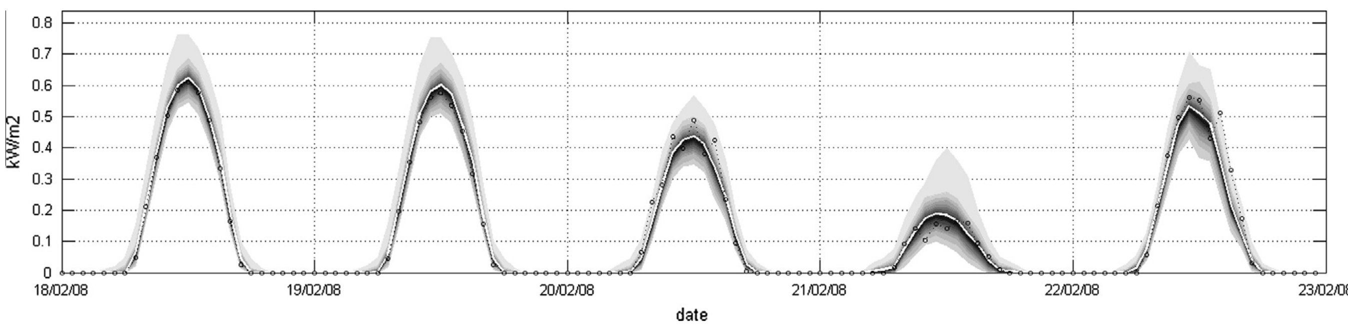


Fig. 13. Prediction intervals from $P(5)$ to $P(100)$ (gray) – forecast $P(60)$ (white) and ground measurements (black dots).

The forecast performance on a fixed horizon, essentially depends on site and year. To compare the accuracy obtained by different models in different sites or years a reference model is used. If the reference model has similar performance (with respect to a specific metric) in two different sites or years then the two weather conditions can be considered comparable. Thus also accuracy of different forecast models calculated by the same metric can be compared. The skill score (Beyer et al., 2009) is less site and year dependent and it allows to evaluate which forecasting model outperforms.

The most common reference model used in the solar forecast sector is the Persistence Model (PM). This is a trivial model that assumes that the forecast weather conditions are the same of the ones of the previous day. Obviously all the forecast models should outperform the persistence. There are several version of PM (Beyer et al., 2009). In this work, to compare the performance of the models to the one reported in Lorenz et al. (2009b), the following PM model is adopted:

$$[Gh(t+1), \ldots Gh_{24}(t+1)] = \langle K_t^*(t)\rangle [Gh_{cs1}(t+1), \ldots Gh_{cs24}(t+1)] \quad (11)$$

where

$\langle K_t^*(t)\rangle$ = daily average of the hourly clear sky index of the day $(t)$.

$[Gh_{cs1}(t+1), \ldots Gh_{cs24}(t+1)]$ = Clear Sky irradiance of the day $(t+1)$.

$Gh_{cs}$ is calculated using the Clear Sky model (Ineichen and Perez, 2002; Reno et al., 2012).

Thus the improvement (skill score with respect to the RMSE metric) can be evaluated for different years with the following formula:

$$\text{Irmse} = 100\left(\frac{\text{RMSE(PM)} - \text{RMSE(model)}}{\text{RMSE(PM)}}\right)\ (\%) \quad (12)$$

## 6. Reliability of the models

To analyze the model dependence on the yearly data used for training, a cross training procedure was adopted. The procedure consisted in developing four ST and four MOSNN models using a different training year, namely: STNN7Tr2008, STNN5Tr2009, STNN7Tr2010, STNN8 Tr2011, and ECMWF-MOSNN7Tr2008, ECMWF-MOSNN6Tr2009, ECMWF-MOSNN10Tr2010, ECMWF-MOSNN14Tr2011. Then for each year used to test, the performance of three models were evaluated. For instance, to forecast the irradiance of 2008, the models trained on 2009, 2010 and 2011 were used.

Fig. 14 shows the maximum difference between the NMAE of the best model and the NMAE of the worst model realized on the test year. It appears that for the ST model such difference reaches 1.7% while for the MOSNN

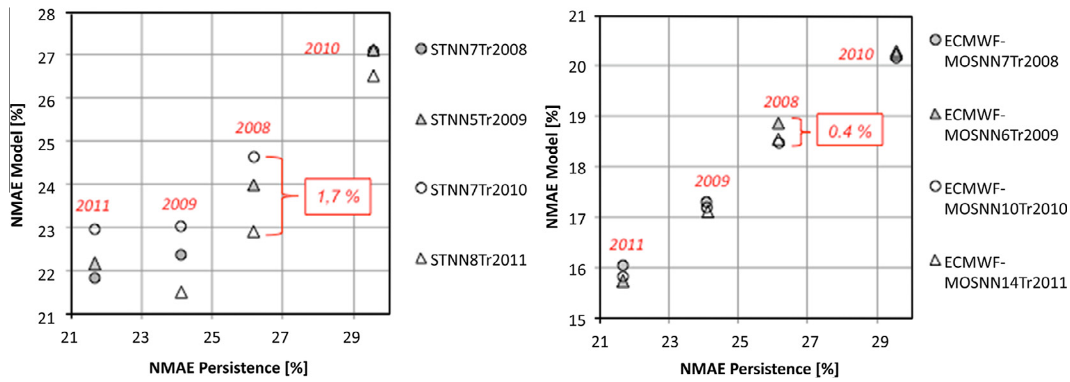


Fig. 14. Normalized mean absolute errors of STNN and ECMWF-MOSNN models for the four years tested.

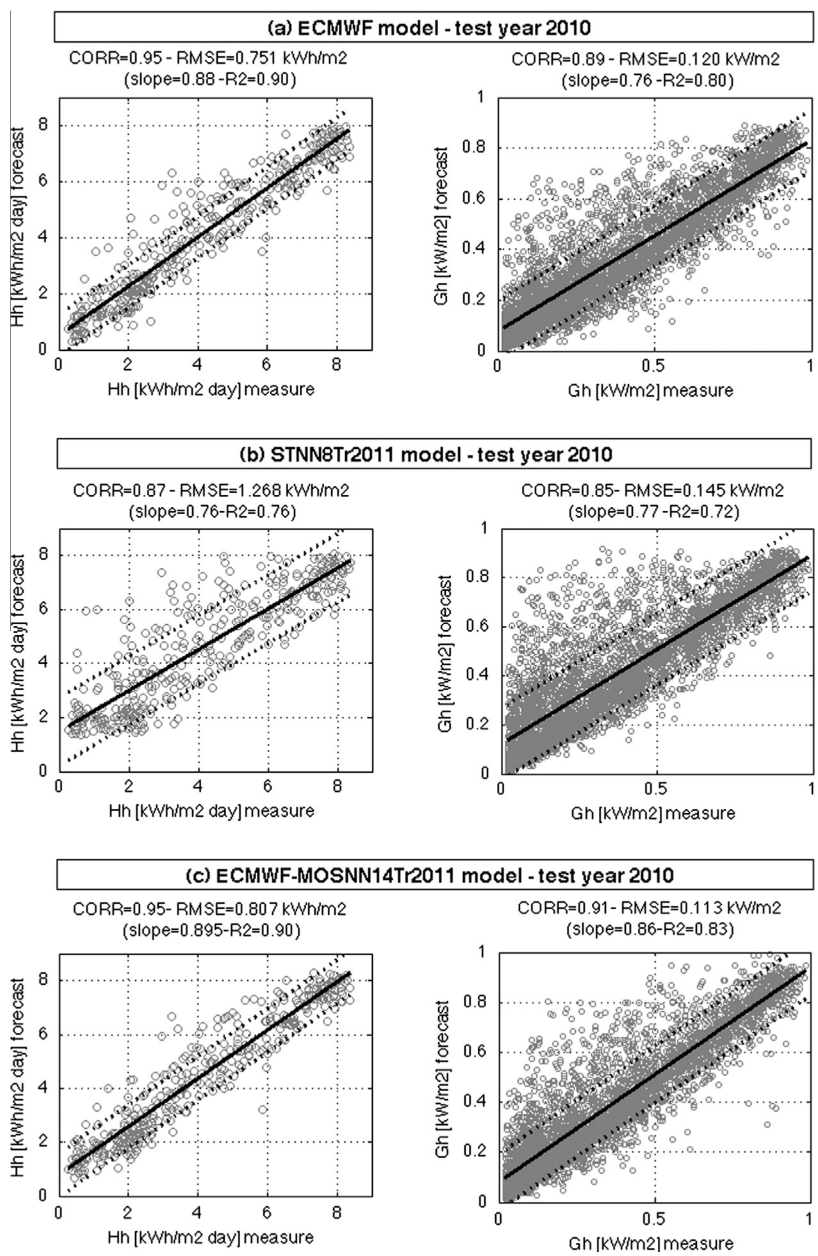


Fig. 15. Scatter plots and Pearson correlation coefficient (CORR) between the measured and forecast on a daily and hourly basis.

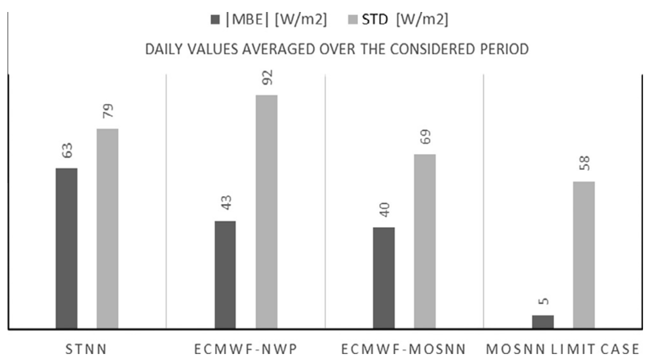


Fig. 16. Daily irradiation and hourly irradiance forecasting errors of different models.

model is lower than 0.5%. Thus the models are reliable since they show just a small dependence on the training years. On the contrary, the models performance depends almost linearly on the persistence model error. Besides it was tested that the performance increased with two year training period while the dependence on the training period decreased.

It should be remarked that the performance of the models (STNN and ECMWF-MOSNN) that will be discussed in the next section, was evaluated as the average accuracy of the three models on the test year. In this way the models performance did not depend on the training dataset.

## 7. Analysis of error sources

From the statistical point of view, two different sources of forecast errors impact the daily MAE: one is in the prediction of the daily irradiation ($H$) and the other is the prediction of the hourly irradiance ($G$) distribution once the irradiation is fixed. Obviously, these sources are not independent. A considerable daily MAE reduction could be achieved if an accurate irradiation forecast is provided, while even improving the ability to forecast the irradiance distribution, no MAE reduction can be reached if the irradiation prediction is not correct. The daily Mean Bias Error (MBE) is the measure of the irradiation forecast capability: $\mathrm{MBE} = \frac{\sum_{i=1}^{n}\left(G_i^m - G_i^f\right)}{n} = \frac{\left(H^m - H^f\right)}{n}$ (where $n$ is the number of diurnal hours) while the daily Standard Deviation of the residuals is the measure of the hourly forecast error: $\mathrm{SDE} = (\mathrm{RMSE}^2 - \mathrm{MBE}^2)^{1/2}$. In the NWP, the irradiance distribution forecast is negatively affected by the spatial and temporal resolution so that it could be efficiently improved by the MOS models.

The scatter plots and the Pearson correlation coefficient allow to point out these two error sources in a more visual way.

Fig. 15 shows the scatter plots of the measured and forecast daily irradiation and hourly irradiance, of the ECMWF, STNN8Tr2011 and ECMWF-MOSNN14Tr2011 models tested on the year 2010. In the graphs also the Pearson correlation coefficient is shown (CORR).

For the ECMWF model a loss of 0.06 in correlation appears passing from daily irradiation ($Hh$) forecast to hourly irradiance forecast ($Gh$), see Fig. 15a. Thus the main source of error of the ECMWF NWP data is in the hourly values prediction, induced by site effects and low output time resolution (3 h interval output data).

On the contrary, the STNN model realizes almost the same correlation in the forecasting of the daily irradiation or of the hourly irradiance as showed in Fig. 15b. Indeed the statistical model mainly fails in the daily irradiation forecast showing a slow reaction to the changing of daily weather conditions. It could not forecast sudden changing in the irradiation since in this case the correlation between the forecast irradiance and the past meteorological parameters used as input, falls down dramatically. On the other hand this model is able to provide a very good forecast of the hourly irradiance using the real day irradiation as input. In this case, it has been proved that the correlation between measured and forecast hourly irradiance grows up to 0.96 with and RMSE around 70–75 $\mathrm{W/m^2}$. This is the limit of accuracy that could be reached by the reported MOSNN model when a perfect daily irradiation forecast is provided (here called: MOSNN limit case).

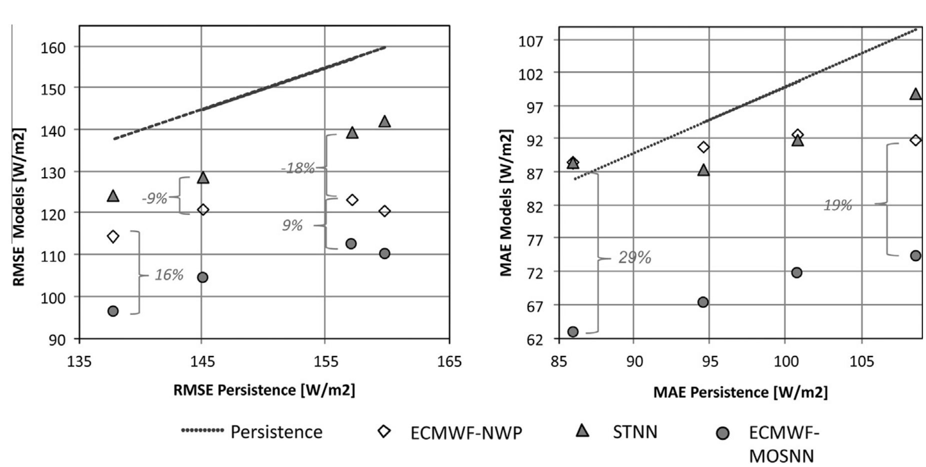


Fig. 17. RMSE and MAE of models vs RMSE and MAE of persistence model.

Table 1
Comparison of accuracy between persistence, ECMWF-NWP and ECMWF-MOSNN.

| Test year | Persistence RMSE ($W/m^2$) | ECMWF-NWP RMSE ($W/m^2$) | ECMWF-MOSNN RMSE ($W/m^2$) | Persistence MAE ($W/m^2$) | ECMWF-NWP MAE ($W/m^2$) | ECMWF-MOSNN MAE ($W/m^2$) | ECMWF-NWP MBE ($W/m^2$) | ECMWF-MOSNN MBE ($W/m^2$) |
|---|---|---|---|---|---|---|---|---|
| 2008 | 157.1<br>41% | 123.2<br>32% | 112.6<br>29% | 100.8<br>26% | 92.7<br>24% | 71.7<br>19% | 15.6<br>4% | −17.9<br>−5% |
| 2009 | 145.0<br>37% | 120.6<br>31% | 104.6<br>27% | 94.5<br>24% | 90.8<br>23% | 67.4<br>17% | 25.8<br>7% | −1.9<br>−0.5% |
| 2010 | 159.7<br>43% | 120.2<br>33% | 110.1<br>27% | 108.6<br>30% | 91.7<br>25% | 74.4<br>20% | 15.7<br>4% | −17.5<br>−5% |
| 2011 | 137.7<br>35% | 114.3<br>29% | 96.4<br>24% | 85.9<br>22% | 88.4<br>22% | 62.9<br>16% | 30.6<br>8% | 5.6<br>1% |

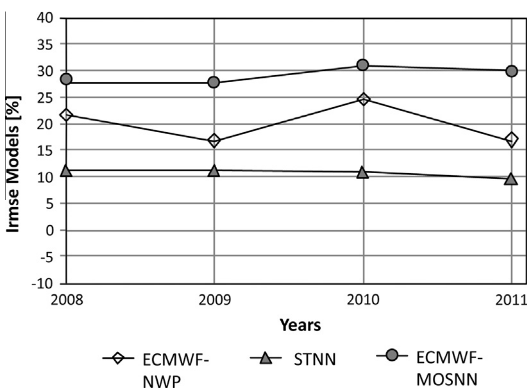


Fig. 18. Improvement with respect to the RMSE for the considered period.

Since the deterministic and statistic approaches have different sources of errors in their forecasting outputs, each method could reduce the error of the other and vice versa. For this reason the MOSNN model always shows the best performance, evidenced in Fig. 15c. The main contribution of the NWP data to the MOSNN performance is related to the good prediction of the daily horizontal irradiation, while the contribution of the statistical ANN model is related to the best hourly irradiance prediction.

Fig. 16 summarizes the above considerations reporting the daily irradiation and the hourly irradiance forecasting error (|MBE| and (STD)) of the different models averaged over the considered period. It is shown that the STNN produces similar error in the prediction of the irradiation and of the irradiance. On the other hand, the greatest error of the ECMWF-NWP is found in the hourly irradiance distribution forecast. The MOSNN provides just a small correction of the irradiation forecast with respect to the NWP, while it greatly improves the irradiance forecast accuracy reaching almost the MOS limit case. Thus to achieve a further improvement of the forecast performance a reduction of the daily bias of the NWP is required. More investigations should be done in this direction.

## 8. Results

### 8.1. Performance analysis

Fig. 17 and Table 1 summarize the main performance indices of the models. It appears that with respect to the NWP, the STNN model realizes a high RMSE (9–18% more) while the MOSNN model obtains an RMSE reduction (9–16% less). In terms of MAE, the NWP and the STNN models show a similar behavior, realizing a MAE even greater than the persistence model for the less variable year 2011. On the other hand the MOSNN model realizes a great MAE reduction with respect to the NWP data (29–19% less).

Fig. 18 shows the improvement of the models with respect to the RMSE of persistence model (Eq. (12)). It can be observed how the improvement is much less time dependent. For the NWP it ranges between 15% and 25%, while for the STNN model is around 10% and for MOSNN model is around 30%.

Lorenz et al. (2009b) find a relative RMSE of different MOS forecasting model ranging from 40% to 60% for the Central European Stations and from 20% to 35% for the South of Spain. The reported results obtained for the Rome Station match these benchmarks since the relative RMSE ranges between 25% and 30%.

In particular Table 2 summarizes the benchmark accuracy values reported by Lorenz et al. (2009b) for Southern Spain and the Swiss stations, compared to the one obtained for ECMWF-MOSNN model for the Rome station. To compare the results, first of all the persistence model accuracy should be analyzed. In terms of RMSE and MAE the persistence model realizes similar values for Rome and for the Swiss stations. This means that Switzerland and Rome present comparable climatic irradiance behavior (with respect to these metrics), and so similar difficulties in solar forecasting can be found. This consideration has also been confirmed by a previous work (Cornaro et al., 2010). Comparing the results, it should be noted that the benchmark models provide a RMSE of 107–122 $W/m^2$ and a MAE of 70–85 $W/m^2$ with a persistence error of 158 $W/m^2$ and

Table 2
Summary of the benchmark accuracy values reported by Lorenz et al. (2009b) for Southern Spain and Swiss stations and MOSNN accuracy for the Rome station.

| | | RMSE ($W/m^2$) | MAE ($W/m^2$) | MBE ($W/m^2$) |
|---|---|---|---|---|
| Southern Spain | Forecast models | 81–124 (20.8–31.7%) | 48–79.8 (12.2–20.4%) | 1–58.9 |
| | Persistence[a] | 125.88 (32.1%) | 65 (16.6%) | 2.44 |
| Rome | ECMWF-MOSNN | 106 (26.7%) | 69 (18.0%) | −7.9 |
| | Persistence[b] | 150 (39.0%) | 97.4 (25.0%) | |
| Switzerland | Forecast models | 107–122 (39.6–45%) | 70–85 (25.8–31.5%) | −1 to −18 |
| | Persistence[a] | 158 (58.4%) | 104 (38.7%) | −17 |

[a] Average performance on different meteorological stations for the period July 2007–June 2008.
[b] Average performance on different years 2008–2011.

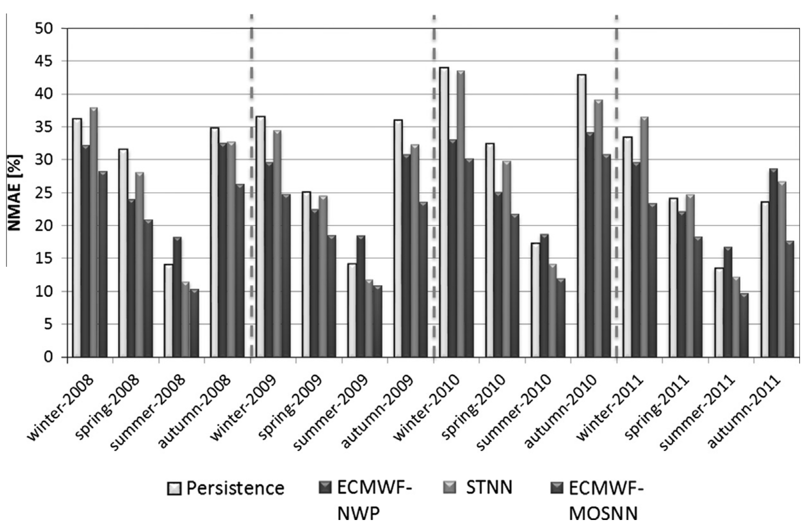


Fig. 19. Seasonal NMAE comparison for the considered period.

Table 3
Seasonal accuracy averaged over the reference periods.

| Season | Persistence | ECMWF-NWP | STNN | ECMWF-MOSNN |
|---|---|---|---|---|
| | NMAE (%) | NMAE (%) | NMAE (%) | NMAE (%) |
| Winter | 38 | 31 | 38 | 27 |
| Spring | 28 | 23 | 27 | 20 |
| Summer | 15 | 18 | 12 | 11 |
| Autumn | 34 | 32 | 33 | 25 |

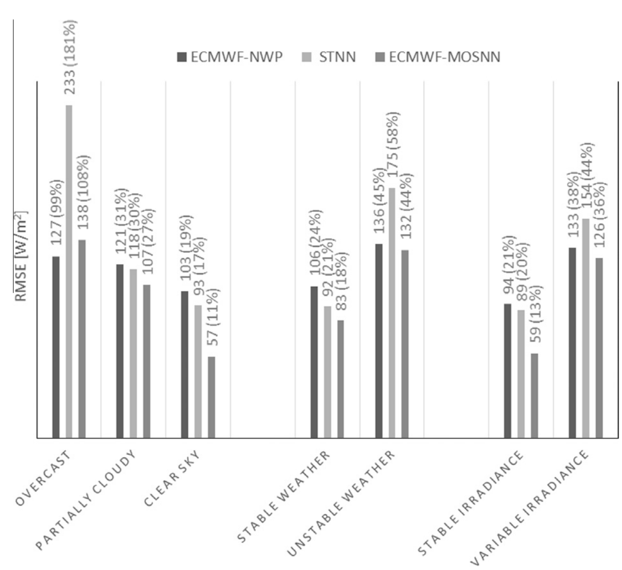


Fig. 20. Models RMSE calculated for different target day features.

104 $W/m^2$. In the year 2008 the ECMWF-MOSNN model realizes a RMSE of 112.6 $W/m^2$ and a MAE of 71.7 $W/m^2$ with a persistence error of 157 $W/m^2$ and 101 $W/m^2$. Thus the results obtained by the MOSNN model can be considered in the range of the one obtained using different approaches for the Swiss stations.

The forecast performance realized by the reported ECMWF-MOSNN model is very similar to the accuracy obtained by the best MOS model, the ECMWF-OL model, developed by Lorenz et al. (2009a,b). On the contrary the

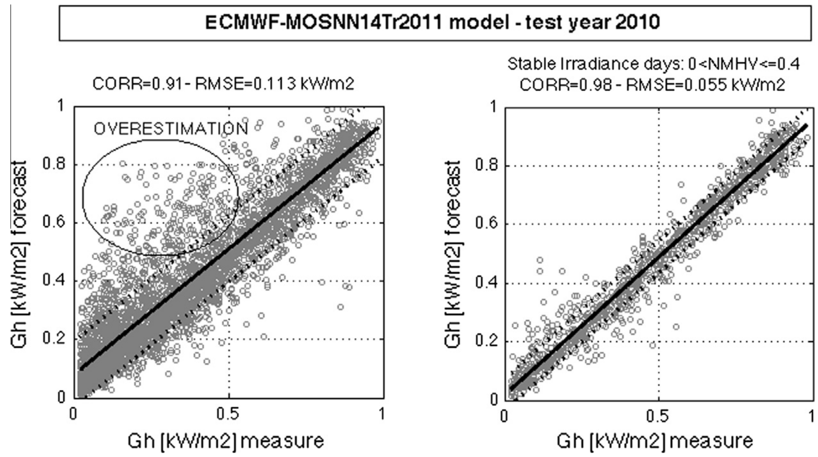


Fig. 21. Correlation obtained for the MOSNN model on all the days (left) and only on stable irradiance days (right).

reported ensemble technique to estimate the prediction interval is not so well performing. Indeed only 58% of the measured irradiance values are found to be inside the $P(100)$–$P(5)$ trajectories, while almost 95% was expected. Thus the prediction intervals are underestimated resulting in a $\Delta G_{rel} = 9\%$ (Eq. (13)). Using the method developed by Lorentz et al. 2009b all the measured values were found inside the prediction intervals but with a $\Delta G_{rel} = 28\%$.

$$\Delta G_{rel} = \sum_{i=1}^{N} [P_i(100) - P_i(5)]/4 \sum_{i=1}^{N} G_i^m \tag{13}$$

The ANN Ensemble does not explore enough prediction trajectories, since the ANN are not able to sensibly modify the daily irradiation values. Indeed all the trajectories of the MOS model provide a daily irradiation near to the one predicted by the NWP. This produces narrow prediction intervals. Further studies should be done to overcome this problem.

### 8.2. Seasonal analysis

Fig. 19 shows the seasonal performance of the models for the years: 2008–2011, while Table 3 reports the seasonal accuracy averaged over the reference periods.

The NWP realizes higher NMAE with respect to the persistence in summer time, due to high errors in hourly irradiance forecast. The STNN model obtains a NMAE comparable to the persistence in Winter, Spring and Autumn. For the same periods the STNN shows worst performance with respect to the NWP, due to the higher errors in the daily irradiation forecast.

The MOSNN model shows always the lower NMAE ranging between 11% in Summer and 27% Winter.

Fig. 20 shows RMSE of the models calculated for the different target day features described in Section 3. As expected, the ECMWF model shows lower performance for clear sky, stable weather and stable irradiance days, since for these days, the hourly irradiance forecasting errors due to low spatial and time resolution have a greater impact on the RMSE. On the contrary the NWP obtains the lower RMSE for the overcast days since in this case the correct daily irradiation prediction is much more important than the forecast of the hourly irradiance distribution. For the opposite reasons the STNN model shows the worst performance in the irradiance prediction of the overcast, unstable weather and variable irradiance days.

Fig. 21 reports the correlation between the MOSNN model results and the measurements for all the days (left) and only for stable irradiance days (right) of the test year. It can be observed that the overestimation data at low irradiance level is almost completely removed in the stable irradiance days. Indeed the model provides the best envelope of the hourly irradiance distribution for a given daily irradiation but cannot forecast the irradiance fluctuation due to clouds motion. Moreover it is more probable to find events with lower irradiance with respect to the predicted value (shading of the sun disc due to clouds) than with higher irradiance (see Fig. 12). This effect produces an irradiance overestimation. This phenomenon does not affect the days with stable irradiance (clear sky or permanently overcast).

## 9. Conclusions

In this paper two models developed to forecast the hourly solar irradiance with 24 h in advance are described. The first one is a statistical model (STNN) that uses only ground measurement data for the prediction. The second one is a Model Output Statistic model (ECMWF-MOS-NN) that corrects the ECMWF-NWP data coming from the European Center of Medium Weather Forecast using ground measurements.

The models are based on ensemble of Artificial Neural Networks (ANN). The master optimization process used to optimize the number of neuron in the hidden layer and to select the ANN Ensemble is reported in detail. The ensemble technique is also used to provide a prediction interval. The models are trained and validated using one year data measured at the ESTER Laboratory of the

University of Rome “Tor Vergata”. A cross-training procedure, based on four years of data, was used to study the dependence of the models performance on the dataset used to train and validate the ANN. It has been proved that the models are reliable and self improving since their performance does not depend on the training year. The models accuracy could be also improved increasing the training period.

The performance of STNN, ECMWF-NWP and ECMWF-MOSNN models were compared to the benchmark persistence model. The statistical model STNN showed greater RMSE than ECMWF-NWP while similar NMAE was found. Even if the MBE of the STNN model was of 1.1% while the MBE of the NWP was of 5.7%, the improvement with respect to the RMSE of the persistence model was around 10% for STNN and 15–25% for the NWP model. This performance is due to different sources of forecast errors. The NWP model provides a very good forecast of the daily irradiation but it fails in the hourly irradiance prediction because of the low spatial and temporal resolution. On the other hand, the ST model is able to provide a good hourly forecast but it could not well predict the daily irradiance in unstable weather conditions. Thus each method contributes to reduce the error of the other and vice versa. For this reason the ECMWF-MOSNN showed the best performance, with a RMSE improvement of 30%, with respect to the persistence model.

Switzerland and Rome present similar difficulties in solar forecasting since the same persistence model accuracy was measured. The results obtained by the MOSNN model (RMSE = 106 W/m$^2$ and MAE = 62 W/m$^2$) can be considered perfectly in the range of the one obtained with different approaches for the Swiss stations (Lorenz et al., 2009b) (RMSE = 107–122 W/m$^2$ and MAE = 70–85 W/m$^2$). While the forecast performance of ECMWF-MOSNN is very similar to the ECMWF-OL model developed by Lorenz et al. (2009a,b), the prediction intervals are not so well estimated. Further investigations should be done to improve the reliability of the prediction intervals.

## Acknowledgements

ECMWF NWP data used in this study have been provided by ECMWF.

We gratefully acknowledge the PV Performance Modeling Collaborative website for providing PV_lib Matlab libraries.

The ESTER facility is part of the Centre for Hybrid and Organic Solar Energy (CHOSE), Italy, partially funded by the Lazio Region.

## References

Beyer, H.G., Polo Martinez, J., Suri, M., Torres, JL., Lorenz, E., Müller, S.C., Hoyer-Klick, C., Ineichen, P.D., 2009. Report on Benchmarking of Radiation Products. Report under Contract No. 038665 of MESoR, 2009. <http://www.mesor.net/deliverables.html> (accessed 01.12.2012).

Cai, T., Duan, S., Chen, C., 2010. Forecasting power output for grid-connected photovoltaic power system without using solar radiation measurement. In: Proceedings of the 2nd International Symposium on Power Electronics for Distributed Generation Systems, PEDG 2010, pp. 773–777.

Cao, J., Lin, X., 2008. Study of hourly and daily solar irradiation forecast using diagonal recurrent wavelet neural networks, 2008. Energy Convers. Manage. 49 (6), 1396–1406.

Chaouachi, A., Kamel, R.M., Ichikawa, R., Hayashi, H., Nagasaka, K., 2009. Neural Network Ensemble-based Solar Power Generation Short-Term Forecasting, Engineering and Technology, 30, World Academy of Science.

Chen, C., Duan, S., Cai, T., Liu, B., 2011. Online 24-h solar power forecasting based on weather type classification using artificial neural network. Sol. Energy 85, 2856–2870.

Cornaro, C., Musella, D., Chianese, D., Friesen, G., Dittmann, S., 2010. Outdoor PV module performance comparison at two different locations. In: Proceedings of ASME-ATI-UIT 2010, Symposium on Thermal and Environmental Issues in Energy Systems, May16–19, 2010, Sorrento, Italy.

Di Piazza, A., Di Piazza, M.C., Vitale, G., 2013. Solar radiation estimate and forecasting by neural networks-based approach. In: Proceedings of 28thEUPVSEC Conference, pp. 3876–3881.

Huang, Y., Lu, J., Liu, C., Xu, X., Wang, W., Zhou, X., 2010. Comparative study of power forecasting methods for PV stations. In: 2010 International Conference on Power System Technology: Technological Innovations Making Power Grid Smarter. Proceedings of POWERCON2010.

Ineichen, P., Perez, R., 2002. A new air mass independent formulation for the Linke turbidity coefficient. Sol. Energy 73, 151–157.

Kleissl, J., 2013. Solar Energy Forecasting and Resource Assessment, first ed. (ISBN 9780123971777).

Lorenz, E., Hurka, J., Heinemann, D., Beyer, H.G., 2009a. Irradiance forecasting for the power prediction of grid connected photovoltaic systems. IEEE J. Sel. Top. Appl. Earth Obs. Remote Sens. 2 (1), 2–10.

Lorenz, E., Remund, J., Müller, S.C., Traunmüller, W., Steinmaurer, G., Pozo, D., Ruiz-Arias, J.A., Lara Fanego, V., Ramirez, L., Romeo, M.G., Kurz, C., Pomares, L.M., Guerrero, C.G., 2009b. Benchmarking of different approaches to forecast solar irradiance. In: Proceedings of the 24th European Photovoltaic Solar 35 Energy Conference 2009; Hamburg, Germany, pp. 4199–4208.

Marquez, R., Coimbra, C.F.M., 2011. Forecasting of global and direct solar irradiance using stochastic learning methods, ground experiments and the NWS database. Sol. Energy 85, 746–756.

Mellit, A., Massi, Pavan A., 2010. A 24-h forecast of solar irradiance using artificial neural network: application for performance prediction of a grid-connected PV plant in Trieste, Italy. Sol. Energy 84, 807–821.

Muller, S.C., Remund, J., 2010. Advances in radiation forecast based on regional weather models MMF and WRF. In: Proceedings 25th EUPVSEC Conference 2010, pp. 4629–4632.

Paulescu, M., Paulescu, E., Gravila, P., Badescu, V., 2013. Weather modeling and forecasting of PV systems operation, first ed. (ISBN 978-1-4471-4649-0).

Perez, R., Moore, K., Wilcox, S., Renné, D., Zelenka, A., 2007. Forecasting solar radiation–preliminary evaluation of an approach based upon the national forecast database. Sol. Energy 81 (6), 809–812.

Perez, R., Kivalov, S., Schlemmer, J., Hemker Jr., K, Rennè, D., Hoff, T.E., 2010. Validation of short and medium term operational solar radiation forecasts in the US. Sol. Energy 84, 2161–2172.

Perez, R., Lorenz, E., Pelland, S., Beauharnois, M., Van Knowe, G., Hemker Jr., K., Heinemann, D., Remund, J., Müller, S.C., Traunmüller, W., Steinmauerg, G., Pozo, D., Ruiz-Arias, J.A., Lara-Fanego, V., Ramirez-Santigosa, L., Gaston-Romero, M., Pomaresk, L.M., 2013. Comparison of numerical weather prediction solar irradiance forecasts in the US, Canada and Europe. Sol. Energy 94, 305–326.

Perotto, A., Pravettoni, M., Maggioni, E., Spada, F., Strepparava, D., 2013. Global irradiance in the southern alpine climate: meteo modelling and statistical post-processing. In: Proceedings of 28thE-UPVSEC2013, pp. 3968–3972.

Photovoltaic and Solar Forecasting: State of the Art. IEA PVPS Task 14, Subtask 3.1. Report IEA-PVPS T14–01: 2013. October 2013 (ISBN 978-3-906042-13-8).

Reno, M., Hansen, C., Stein, J., 2012. Global Horizontal Irradiance Clear Sky Models: Implementation and Analysis, Sandia National Laboratories, SAND2012-2389.

Spena, A., Cornaro, C., Serafini, S., 2008. Outdoor ESTER test facility for advanced technologies PV modules. In: Proceedings of the 33rd IEEE Photovoltaic Specialists Conference, San Diego.

Statistical data from the Italian Manager of Electrical Services (GSE): "Solare Fotovoltaico – Rapporto Statistico 2012". <http://www.gse.it/it/Statistiche/RapportiStatistici/Pagine/default.aspx>.

Statistical data from the Italian Manager of the National Electrical Transmission Grid (Terna): "produzione 2012". <http://www.terna.it/default/Home/SISTEMA_ELETTRICO/statistiche/dati_statistici.aspx>.

Traunmüller, W., Steinmaurer, G., 2010. Solar irradiance forecasting, benchmarking of different techniques and applications of energy meteorology. In: Proceedings of the EuroSun 2010 Conference, September 28–October 1, 2010, Graz, Austria.

Voyant, C., Randimivololona, P., Nivet, M.L., Poli, C., Muselli, M., 2013. Twenty four hours ahead global irradiation forecasting using multi-layer perceptron. Meteorol. Appl.. http://dx.doi.org/10.002/met.1387.

Wang, S., Zhang, N., Zhao, Y., Zhan, J., 2011. Photovoltaic system power forecasting based on combined grey model and BP neural network. In: ICECE 2011 Proceedings, pp. 4623–4626.

Wang, F., Mi, Z., Su, S., Zhao, H., 2012. Short-term solar irradiance forecasting model based on artificial neural network using statistical feature parameters. Energies 5, 1355–1370.

Yona, A., Senjyu, T., Saber, A.Y., Funabashi, T., Sekine, H., Kim, C., 2008. Application of neural network to 24 h ahead generating power forecasting for PV system. In: Proceedings of IEEE Power and Energy Society 2008 General Meeting: Conversion and Delivery of Electrical Energy in the 21st Century, PES.